

Giant magneto-drag in graphene at charge neutrality

M. Titov,¹ R. V. Gorbachev,^{2,3} B. N. Narozhny,⁴ T. Tudorovskiy,¹ M. Schütt,⁵ P. M. Ostrovsky,^{6,5,7} I. V. Gornyi,^{5,8} A. D. Mirlin,^{5,4,9} M. I. Katsnelson,¹ K. S. Novoselov,² A. K. Geim,^{2,3} and L. A. Ponomarenko²

¹Radboud University Nijmegen, Institute for Molecules and Materials, NL-6525 AJ Nijmegen, The Netherlands

²School of Physics and Astronomy, University of Manchester, Manchester M13 9PL, UK

³Centre for Mesoscience and Nanotechnology, University of Manchester, Manchester M13 9PL, UK

⁴Institut für Theorie der Kondensierten Materie and DFG Center for Functional Nanostructures, Karlsruher Institut für Technologie, 76128 Karlsruhe, Germany

⁵Institut für Nanotechnologie, Karlsruhe Institute of Technology, 76021 Karlsruhe, Germany

⁶Max-Planck-Institut für Festkörperforschung, Heisenbergstr. 1, 70569, Stuttgart, Germany

⁷L.D. Landau Institute for Theoretical Physics RAS, 119334 Moscow, Russia

⁸A.F. Ioffe Physico-Technical Institute, 194021 St. Petersburg, Russia

⁹Petersburg Nuclear Physics Institute, 188350 St. Petersburg, Russia

(Dated: December 2, 2018)

We report experimental data and theoretical analysis of Coulomb drag between two closely positioned graphene monolayers in weak magnetic field. Close enough to the neutrality point, coexistence of electrons and holes in each layer leads to a dramatic increase of the drag resistivity. Away from charge neutrality, we observe non-zero Hall drag. The observed phenomena are explained by decoupling of electric and quasiparticle currents which are orthogonal at charge neutrality. The sign of magneto-drag depends on the energy relaxation rate and geometry of the sample.

PACS numbers: 72.80.Vp, 73.50.Jt, 73.22.Pr, 73.50.-h

Recent measurements [1] of frictional drag in graphene-based double-layer devices revealed the unexpected phenomenon of giant magneto-drag at the charge neutrality point. Applying external magnetic fields as weak as 0.1-0.3 T results in the reversal of the sign and a dramatic enhancement of the amplitude of the drag resistance. If the device is doped away from charge neutrality, the impact of such a weak field on the drag resistance is very modest. The observed effect weakens at low temperatures, hinting at the classical origin of the phenomenon.

In this Letter we report experimental data on longitudinal and Hall drag resistivity in isolated graphene layers separated by a 1 nm thick boron-nitride (hBN) spacer. The observed effects are explained in terms of coexisting electron and hole liquids in each layer [2, 3]. This theory is based on the hydrodynamic description of transport in graphene derived in Refs. 4–6 using the quantum kinetic equation framework [7, 8]. It provides a simplified description of the magneto-drag effect while capturing the essentially classical physics of the phenomenon [9]. The effect can be traced back to the fact that the Lorentz force in the electronic band is opposite to that in the hole band, which is also the reason for the anomalously large Nernst effect [10, 11] and vanishing Hall effect at charge neutrality.

The classical mechanism behind the giant magneto-drag is illustrated in Fig. 1. The upper panel shows two *infinite* graphene layers at charge neutrality. The driving electric current \mathbf{j}_1 in the active layer corresponds to the counter-propagating flow of electrons and holes with zero total momentum due to exact electron-hole symmetry (hence, in the absence of additional correlations there is no drag at the Dirac point [5, 12–15]). In a weak

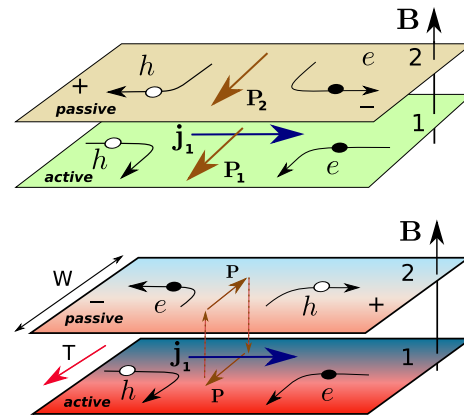


FIG. 1: (Color online) Mechanism of magneto-drag at charge neutrality. Upper panel: in an infinite system quasi-particle currents in the two layers (denoted by \mathbf{P}_i) flow in the same direction, leading to *positive* drag. Lower panel: in a thermally isolated system no net heat flow is possible; the quasi-particle currents in the two layers have opposite directions yielding *negative* drag.

magnetic field, electrons and holes are deflected by the Lorentz force and drift in the same direction. The resulting quasi-particle flow, \mathbf{P}_1 , carries a non-zero net momentum in the direction perpendicular to the charge flow, \mathbf{j}_1 . The momentum transfer by the interlayer Coulomb interaction induces the quasi-particle current \mathbf{P}_2 in the same direction as \mathbf{P}_1 . The Lorentz forces acting on both types of carriers in the passive layer drive the charge flow in the direction opposite to \mathbf{j}_1 . If the passive circuit is open, this current is compensated by a finite drag voltage, yielding a *positive* drag resistivity.

This mechanism of magneto-drag at charge neutrality

is closely related to the anomalous Nernst effect in single-layer graphene [4, 10, 11]. Indeed, the quasi-particle current is proportional to the heat current at the Dirac point. A similar mechanism, where the role of \mathbf{P}_i is played by a spin current, has been proposed in Ref. [16] as a possible explanation for a giant non-local magnetoresistance at charge neutrality.

The above argument describes the steady state in the infinite system where all physical quantities are homogeneous in real space. This is not the case in a relatively small mesoscopic sample. Whether a particular sample should be considered “small” or “large” is determined by comparing the sample size to the typical length scale corresponding to the leading relaxation process. At high enough temperatures, the heat currents are most efficiently relaxed by electron-phonon scattering, which we describe in this Letter by the phenomenological length scale ℓ_{ph} [17, 18].

In a finite system, the quasi-particle currents must vanish at the boundaries. For $W \gg \ell_{\text{ph}}$, the quasi-particle current and density is homogeneous in the bulk and the system remains effectively infinite.

For $W \ll \ell_{\text{ph}}$, the currents \mathbf{P}_i acquire a dependence on the coordinate y . In this case energy conservation dictates that $\mathbf{P}_2(y) = -\mathbf{P}_1(y)$. As the result the electric charge in the passive layer tends to flow *in the same direction* as \mathbf{j}_1 , see Fig. 1. Thus, the drag is *negative*, which is the conventional sign for the Coulomb drag in a system with the same type of charge carriers.

In order to test the above ideas, we perform new measurements of the drag effect in magnetic field which are illustrated in Fig. 2. The experiments are carried out on graphene double-layer structure with 1 nm hBN spacer and two electrostatic gates. The schematics of the experiment is shown in the inset of the panel D in Fig. 2. The same device was used in Ref. 1 for drag measurements in zero magnetic field.

The map for the drag resistivity, $\rho_{xx}^D(V_T, V_B)$, is shown in Fig. 2, panel A at $T = 240$ K. The main difference compared to zero field experiment reported earlier [1] is large negative drag at the double neutrality point. A dramatic change in drag resistivity with the applied magnetic field is shown in more details in Fig. 2, panel B at a lower temperature, $T = 160$ K. To ensure same charge densities n_1 and n_2 in the top and bottom layers, we sweep both gates simultaneously along the line connecting the bottom left and top right corners of the map. The experiment shows a large negative peak in ρ_{xx}^D at the double neutrality point, $n_1 = n_2 = 0$, as expected for a small sample (see above); in our device both layers have the width $W \approx 2\mu\text{m}$ and sufficiently resistive contacts.

In addition to the longitudinal drag resistivity we also measure the Hall drag resistivity, $\rho_{xy}^D(V_T, V_B)$, shown in Fig. 2, panel C at $T = 240$ K as a function of the top and bottom gate voltages. Due to the low density of states in graphene and the small separation between lay-

ers (in this experiment $d \approx 1$ nm), the relationship between gate voltages and charge densities is rather non-trivial. To identify sign of charge carriers at each point in Fig. 2, panel C, we also measured resistivity maps for both layers. Since the resistance of graphene is peaked at charge neutrality, tracking the position of the resistivity maximum gives the lines which divide the map into the electron- and hole-doped parts. Such lines are shown in both maps, see Fig. 2, panels C and A. The observed Hall drag resistance is large when one of the layers is close to neutrality point and vanishes if two layers have the same charge densities with opposite signs (a white line running from the top left to bottom right corner).

We now turn to the theoretical description of the drag effect. Consider first the Drude model for electrons and holes in the two layers:

$$e\mathbf{E}_1 + e[\mathbf{v}_{1e} \times \mathbf{B}] = \mathbf{F}_{1e} + e\mathbf{v}_{1e}/M_1, \quad (1a)$$

$$-e\mathbf{E}_1 - e[\mathbf{v}_{1h} \times \mathbf{B}] = \mathbf{F}_{1h} + e\mathbf{v}_{1h}/M_1, \quad (1b)$$

$$e\mathbf{E}_2 + e[\mathbf{v}_{2e} \times \mathbf{B}] = \mathbf{F}_{2e} + e\mathbf{v}_{2e}/M_2, \quad (1c)$$

$$-e\mathbf{E}_2 - e[\mathbf{v}_{2h} \times \mathbf{B}] = \mathbf{F}_{2h} + e\mathbf{v}_{2h}/M_2. \quad (1d)$$

The velocities, \mathbf{v}_{ia} with $i = 1, 2$ and $a = e, h$, are the mean velocities of electrons and holes in the layer i , $\mathbf{E}_{1,2}$ and \mathbf{B} are the electric and magnetic fields, e is the elementary charge, and $M_{1,2}$ are the carrier mobilities due to scattering on impurities. The electric \mathbf{j}_i and quasi-particle \mathbf{P}_i currents are related to \mathbf{v}_{ia} by [2]

$$\mathbf{j}_i = e(n_{ie}\mathbf{v}_{ie} - n_{ih}\mathbf{v}_{ih}), \quad \mathbf{P}_i = n_{ie}\mathbf{v}_{ie} + n_{ih}\mathbf{v}_{ih}, \quad (2)$$

with the electron and hole concentrations $n_{ie(h)} = \int_0^\infty d\varepsilon \nu(\varepsilon) [e^{(\varepsilon \mp \mu_i)/T} + 1]^{-1}$. Here $\nu(\varepsilon) = 2|\varepsilon|/\pi(\hbar v)^2$ is the density of states in graphene (disregarding the magnetic field), and μ_i are the chemical potentials measured from the Dirac point. The total charge and quasi-particle densities are defined as $n_i = n_{ie} - n_{ih}$ and $\rho_i = n_{ie} + n_{ih}$.

In general, the frictional force acting on each type of carriers can be represented by the sum

$$\mathbf{F}_{ia} = \hbar \sum_{jb} [\gamma_{ij}^{ab} n_{jb}(\mathbf{v}_{ia} - \mathbf{v}_{jb}) + \tilde{\gamma}_{ij}^{ab} n_{jb}(\mathbf{v}_{ia} + \mathbf{v}_{jb})], \quad (3)$$

where the coefficients $\tilde{\gamma}$ appear in monolayer graphene due to the absence of Galilean invariance. The expression (3) can be obtained by solving the quantum kinetic equation in the hydrodynamic approximation [19]. The dimensionless coefficients γ_{ij}^{ab} and $\tilde{\gamma}_{ij}^{ab}$ are related to microscopic collision rates [4–7].

For $n_i = 0$, the first term in Eq. (3) simplifies to

$$\mathbf{F}_{1a} = -\mathbf{F}_{2a} = \hbar \gamma (\mathbf{P}_1 - \mathbf{P}_2), \quad (4)$$

where $\gamma = \hbar/T\tau_P$, with τ_P^{-1} being the momentum relaxation rate. The second term in Eq. (3) renormalizes the mobilities [5, 7, 8]. The model (1) with the force (4) also describes the case $\mu_1 = \mu_2 \gg T$, where $\gamma = \hbar/\mu_1\tau_P$.

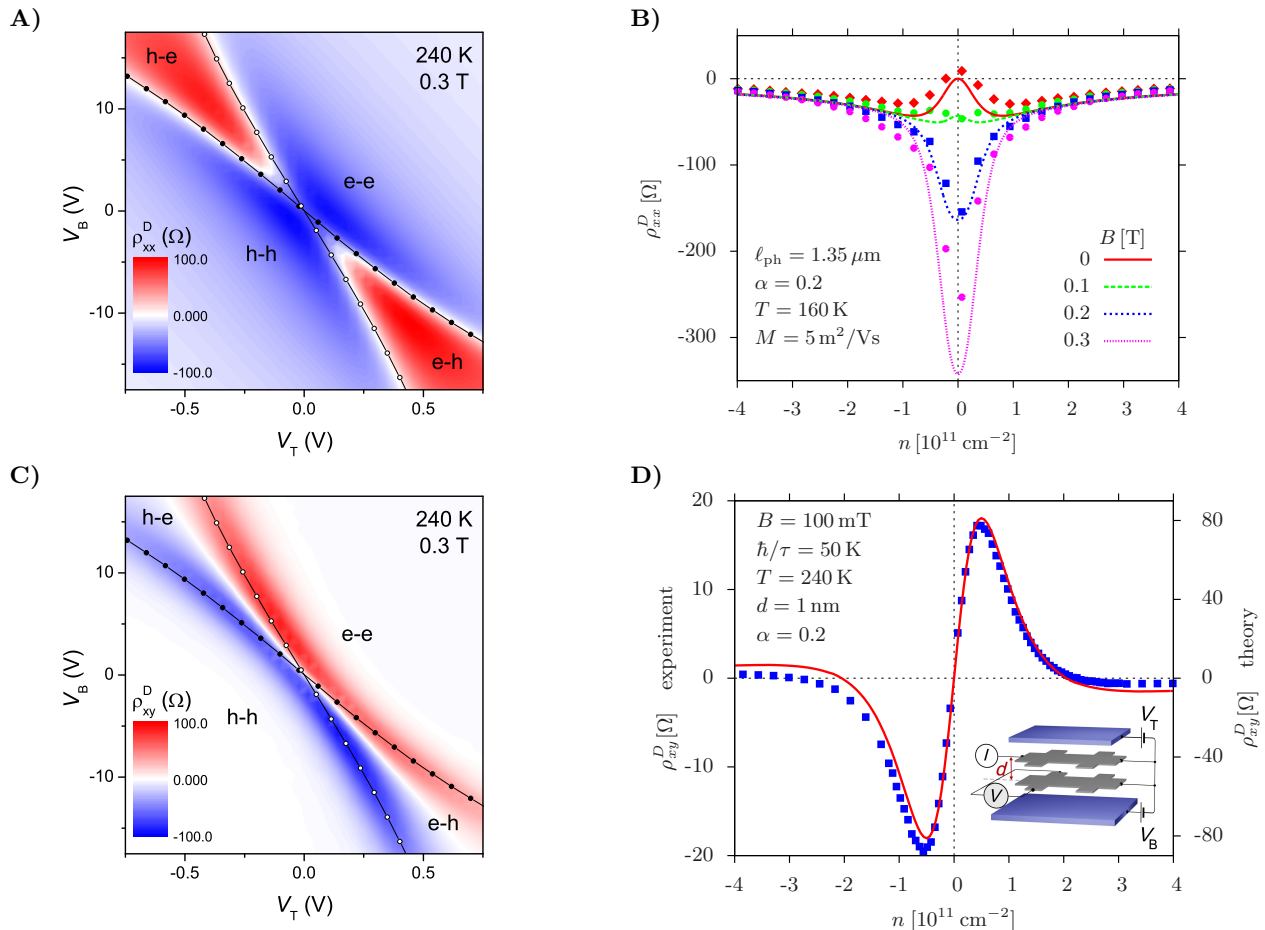


FIG. 2: (Color online) Panel A: Longitudinal drag resistivity in magnetic field as a function of the top and bottom gate voltages. Lines track positions of the neutrality points in top (open symbols) and bottom (closed symbols) layers and divide the map into four regions with distinct signs of charge carriers (e-e, h-h, e-h, h-e). Panel B: Magneto-drag for equal charge densities $n_1 = n_2 = n$. Solid symbols represent the experimental data. The lines show the results of the proposed theory (see main text for details). Different colors correspond to different values of the magnetic field. The electron-phonon relaxation length ℓ_{ph} was determined by fitting. Panel C: The map of Hall drag resistivity as function of top and bottom gate voltages. The white diagonal corresponds to vanishing Hall drag for $n_1 = -n_2$. The lines with open and closed symbols indicate neutral states of the top and bottom layers, respectively. Panel D: The experimental data (blue squares, left axis) and theoretical plot (red solid line, right axis) for the Hall drag resistivity for equal charge densities $n_1 = n_2 = n$. The theoretical curve is calculated from the phenomenological model (1) with the frictional force (3) as derived [9] from the quantum kinetic equation in the hydrodynamic approximation [5] using the dynamic RPA screening and the mean impurity scattering time τ . Note the sign change at $n \approx \pm 2 \times 10^{11} \text{ cm}^{-2}$. Inset: schematics of Hall drag measurements in double layer system. The charge density is controlled by voltages V_T and V_B applied to the top and bottom gate, respectively.

For strongly-doped graphene, $\mu_i \gg T$, the quasi-particle current and density are obsolete: $\mathbf{P}_i = \mathbf{j}_i/e$ and $\rho_i = n_i$. Equations (1) may then be reduced to the standard Drude model yielding the vanishing Hall drag resistivity $\rho_{xy}^D = -E_{2y}/j_{1x} = 0$ and conventional drag, $\rho_{xx}^D = E_{2x}/j_{1x} = -\hbar\gamma/e^2$, which show negligible dependence on the magnetic field [20].

In contrast, at charge neutrality the quasi-particle and charge degrees of freedom are decoupled. The quasi-particle density for $n_i = 0$ is determined by the temperature as $\rho_i = \rho_0 = \pi T^2/3(\hbar v)^2$, while the electric and quasi-particle currents \mathbf{j}_1 and \mathbf{P}_i become orthogonal, as shown in Fig. 1.

Rewriting Eqs. (1), (4) in terms of currents (2) and excluding \mathbf{P}_i , we obtain the resistivity tensor. At charge neutrality, $n_i = 0$, the longitudinal drag resistivity is peaked and its value is given by the expression

$$\rho_{xx}^D = \frac{\hbar\gamma}{e^2} \frac{B^2 M_1 M_2}{1 + \hbar\gamma\rho_0(M_1 + M_2)/e}, \quad n_i = 0, \quad (5)$$

which describes positive drag in an infinite system in agreement with the qualitative picture illustrated in Fig. 1, upper panel. In the limit of weak interaction, $\gamma M T^2 \ll \hbar e v^2$, the result (5) can be obtained from the standard perturbative approach [13] modified for graphene in a classical magnetic field.

From Eqs. (1) and (3) we also calculate the Hall drag resistivity ρ_{xy}^D . The frictional force (3) is derived [9] from the quantum kinetic equation in the hydrodynamic approximation [5] using the dynamic RPA screening and the mean impurity scattering time τ . The resulting dependence of the Hall drag on the charge density, $n = n_1 = n_2$, are shown in Fig. 2, panel D along with the corresponding experimental data without any fitting. The value of the scattering time τ is determined from the single-layer resistivity measured in experiment and we have used the most plausible estimate for the value of the effective electron-electron interaction strength, $\alpha \approx 0.2$, in graphene on hBN. The theory also predicts the vanishing Hall drag for the case of oppositely doped layers, $n_1 = -n_2$, as well as the additional zero in the Hall drag at some finite value of the charge density, which agrees with the experimental data shown in Fig. 2, panel C,

At the same time, the large negative peak in the longitudinal drag resistivity at the double neutrality point, see Fig. 2, panel B, suggests that the sample width, $W \approx 2 \mu\text{m}$ is relatively small as compared to ℓ_{ph} at $T = 160 \text{K}$, see Fig. 1, lower panel. To account for the finite width of the sample, we need to re-write the equations (1) in terms of the currents \mathbf{j}_i and \mathbf{P}_i and allow for the spatially varying quasi-particle density, ρ_i (where we need to use the continuity equation). The resulting model for the first layer at charge neutrality reads (for the second layer one has to replace the index 1 with 2)

$$-\bar{T}_1 \nabla \rho_1 + en_1 \mathbf{E}_1 + [\mathbf{j}_1 \times \mathbf{B}] = \rho_1 \mathbf{F}_1 + e \mathbf{P}_1 / M_1, \quad (6a)$$

$$e \rho_1 \mathbf{E}_1 + e[\mathbf{P}_1 \times \mathbf{B}] = n_1 \mathbf{F}_1 + \mathbf{j}_1 / M_1, \quad (6b)$$

$$\nabla \mathbf{P}_1 = -(\rho_1 - \rho_0) / \tau_{\text{ph}} - (\rho_1 - \rho_2) / \tau_{\text{Q}}. \quad (6c)$$

Here $\bar{T}_1 = 2T \ln(2 \cosh \mu_1 / 2T)$ is the mean quasi-particle energy. The continuity equation for the quasi-particle current (6c) includes relaxation by the electron-hole recombination [2], with τ_{ph}^{-1} describing the energy loss from the system, which at high enough temperatures is dominated by phonon scattering [17], and τ_{Q}^{-1} describing the quasiparticle imbalance relaxation due to the interlayer Coulomb interaction. Note, that the interlayer interaction does not lead to relaxation of the total quasi-particle current $\mathbf{P}_1 + \mathbf{P}_2$, which therefore vanishes if $\tau_{\text{ph}}^{-1} = 0$. Near the Dirac point, energy and momentum relaxation rates coincide (in particular, $\tau_{\text{Q}} \sim \tau_{\text{P}}$). In doped graphene ($\mu \gg T$), the recombination rates are exponentially suppressed.

The continuity equation for the electric current simply reads $\nabla \mathbf{j}_i = 0$, hence $\mathbf{j}_i = (j_i(y), 0)$. Within linear response, the density ρ_i has to be substituted by the equilibrium value ρ_0 in the products $\rho_i \mathbf{F}$ and $\rho_i \mathbf{E}$. This way we obtain the linear system of differential equations on the functions $P_{iy}(y)$, $j_{1x}(y)$, and $\rho_i(y)$. Since the charge current acquires the dependence on the transverse coordinate, we define $\rho_{xx}^D = E_{2x} / \langle j_{1x} \rangle$, where $\langle j_{1x} \rangle = W^{-1} \int_0^W j_{1x} dy$.

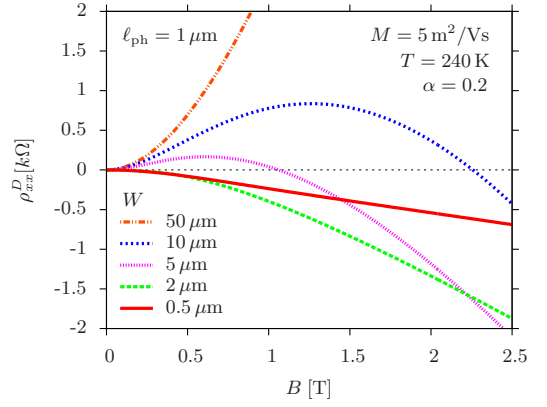


FIG. 3: (Color online) The magnetic field dependence of the longitudinal drag resistivity at the neutrality point calculated from Eq. (7). The positive sign of the magneto-drag in weak fields corresponds to the limit $W \gg 2\ell_{\text{ph}}$, where $\ell_{\text{ph}} \approx 1 \mu\text{m}$ for the parameters of the plot. The magnetic field dependence of scattering rates is disregarded in the plot.

Solving the above differential equations for $n_i = 0$ and $M_i = M$, we find the drag resistivity

$$\rho_{xx}^D = \frac{\rho_{xx}^{(0)}}{2} \left[F(0,0) - F \left(\frac{\hbar\gamma}{e^2 \rho_{xx}^0}, \frac{\tau_{\text{ph}}}{\tau_{\text{Q}}} \right) \right], \quad (7a)$$

$$F(X,Y) = \frac{1 + 2X + (MB)^2}{1 + 2X + (MB)^2 \frac{\tanh \Theta(X,Y)}{\Theta(X,Y)}}, \quad (7b)$$

$$\Theta(X,Y) = \frac{W}{2\ell_{\text{ph}}} \sqrt{(1 + 2X + (MB)^2)(1 + Y)}, \quad (7c)$$

where $\rho_{xx}^{(0)} = 1/eM\rho_0$ is the single-layer resistivity in the absence of magnetic field and $\ell_{\text{ph}} = \sqrt{MT}\tau_{\text{ph}}/e$ is the phonon-scattering length. In the weak-field limit, $MB \ll 1$, and for $W \gg \ell_{\text{ph}}$, the magneto-drag (7) is positive and we reproduce the result (5). In the absence of phonons, $\tau_{\text{ph}} \rightarrow \infty$, i.e. for the thermally insulated system, the drag at the Dirac point is always negative, in agreement with the qualitative picture of Fig. 1.

The result (7) is illustrated in Fig. 3, where we plot ρ_{xx}^D as a function of magnetic field for different values of the sample width choosing realistic values for the model parameters $T = 240 \text{K}$, $M = 5 \text{m}^2/\text{Vs}$, and $\ell_{\text{ph}} = 1 \mu\text{m}$.

For doped graphene, we have solved the model Eqs. (6) numerically. The density dependence of the drag resistivity in magnetic field for $T = 160 \text{K}$ is shown in Fig. 2, panel B along with the experimental data. The collapse of the theoretical curves calculated for different values of the magnetic field is an artifact of the phenomenological model [17], which is most reliable near charge neutrality. The numerical solution also shows the suppression of the Hall drag as compared to the model (1) explaining the factor of 4 difference between the theory and experiment in Fig. 2D. Based on these results, we predict that in wider samples, the giant magneto-drag at the Dirac point should become positive. We also speculate that

the magneto-drag at the double Dirac point may become positive in stronger fields due to the magnetic-field dependence of the scattering times τ_Q , τ_P , and τ_{ph} .

In conclusion, we have measured the longitudinal and Hall drag resistivity in double-layer graphene and provided a theoretical description of the observed effects. The giant magneto-drag at the neutrality point appears due to the presence of two types of carriers (electrons and holes), which in weak magnetic fields experience a unidirectional drift orthogonal to the driving current. This effect is specific to the neutrality point, where non-zero drag appears despite the exact electron-hole symmetry. The present theory does not rely on the Dirac spectrum in graphene, but is equivalent to the microscopic theory [5, 9] at and far away from the charge neutrality thus capturing the essential physics of magneto-drag. For a more accurate description of the effect at intermediate densities, the microscopic theory should be formulated on the basis of the kinetic equation [19].

We are grateful to the Royal Society, the Körber Foundation, the Office of Naval Research, the Air Force Office of Scientific Research, the Engineering and Physical Sciences Research Council (UK), Stichting voor Fundamenteel Onderzoek der Materie (FOM, the Netherlands), DFG SPP 1459 and BMBF for support.

Upon completion of this manuscript, we became aware of a related work by Song and Levitov [21].

[1] R.V. Gorbachev, A.K. Geim, M.I. Katsnelson, K.S. Novoselov, T. Tudorovskiy, I.V. Grigorieva, A.H. MacDonald, K. Watanabe, T. Taniguchi, L.A. Ponomarenko, *Nature Phys.* **8**, 896 (2012).
 [2] M.S. Foster and I.L. Aleiner, *Phys. Rev. B* **79**, 085415 (2009).
 [3] D. Svintsov, V. Vyurkov, S. Yurchenko, T. Otsuji, and V. Ryzhii, *J. Appl. Phys.* **111**, 083715 (2012).
 [4] M. Müller and S. Sachdev, *Phys. Rev. B* **78**, 115419 (2008); M. Müller, L. Fritz, and S. Sachdev, *ibid*, 115406 (2008).
 [5] M. Schütt, P. M. Ostrovsky, M. Titov, I.V. Gornyi, B.N. Narozhny, and A.D. Mirlin, *Phys. Rev. Lett.* **110**, 026601 (2013); M. Schütt, PhD thesis (2013).
 [6] J. Lux and L. Fritz, *Phys. Rev. B* **86**, 165446 (2012).
 [7] L. Fritz, J. Schmalian, M. Mueller, and S. Sachdev, *Phys. Rev. B* **78**, 085416 (2008); M. Müller, J. Schmalian, and L. Fritz, *Phys. Rev. Lett.* **103**, 025301 (2009).

[8] A.B. Kashuba, *Phys. Rev. B* **78**, 085415 (2008).
 [9] The hydrodynamic description of drag in graphene derived in Ref. 5 was justified by the singular behavior of the collision integral due to kinematics of Dirac fermions. This singularity leads to the fast unidirectional thermalization and allows one to select the relevant eigenmodes of the collision integral [4, 7]. Projecting the collision integral onto the momentum and velocity modes, one arrives at the effective model in terms of energy and electric currents, which is equivalent to Eq. (1) with the generalized force (4). At the Dirac point the energy current is equivalent to the quasi-particle current \mathbf{P} .
 [10] Y.M. Zuev, W. Chang, and P. Kim, *Phys. Rev. Lett.* **102**, 096807 (2009).
 [11] P. Wei, W.Z. Bao, Y. Pu, C.N. Lau, and J. Shi, *Phys. Rev. Lett.* **102**, 166808 (2009).
 [12] W. Tse, B.Yu-K. Hu, and S. Das Sarma, *Phys. Rev. B* **76**, 081401 (2007).
 [13] B.N. Narozhny, M. Titov, I.V. Gornyi, and P.M. Ostrovsky, *Phys. Rev. B* **85**, 195421 (2012).
 [14] M. Carrega, T. Tudorovskiy, A. Principi, M.I. Katsnelson, and M. Polini, *New J. Phys.* **14**, 063033 (2012).
 [15] B. Amorim and N.M.R. Peres, *J. Phys.: Cond. Mat.* **24**, 335602 (2012).
 [16] D.A. Abanin, S.V. Morozov, L.A. Ponomarenko, R.V. Gorbachev, A.S. Mayorov, M.I. Katsnelson, K. Watanabe, T. Taniguchi, K.S. Novoselov, L.S. Levitov, and A.K. Geim, *Science* **332**, 328 (2011).
 [17] The lowest order phonon contribution to the electron-hole recombination in graphene is kinematically forbidden. There are, however, many possible mechanisms of recombination [2, 18], all of them involving phonons. Therefore, we phenomenologically regard the time and length scale of electron and hole recombination as ℓ_{ph} and τ_{ph} . Moreover, the microscopic theory [5, 19] is formulated in terms of energy currents rather than quasiparticle currents. In graphene the energy current is equal to the total momentum [5]. Therefore, the corresponding relaxation processes do not require recombination and can be directly attributed to phonons. At the same time, the hydrodynamic description in terms of the energy currents yields only the power-law decay of the magneto-drag at $\mu_i \gg T$, in contrast to the exponential collapse shown in Fig. 2, panel B.
 [18] J.C.W. Song, M.Y. Reizer, and L.S. Levitov, *Phys. Rev. Lett.* **109**, 106602 (2012).
 [19] M. Schütt *et al.*, in preparation.
 [20] A.-P. Jauho and H. Smith, *Phys. Rev. B*, **47** 4420 (1993); K. Flensberg, B.Y. Hu, A.-P. Jauho, J.M. Kinaret, *Phys. Rev. B* **52**, 14761 (1995); A. Kamenev and Y. Oreg, *Phys. Rev. B* **52**, 7516 (1995).
 [21] J.C.W. Song and L.S. Levitov, arXiv:1303.3529 (2013).